Available online at www.sciencedirect.com

ScienceDirect

journal homepage: www.elsevier.com/locate/he

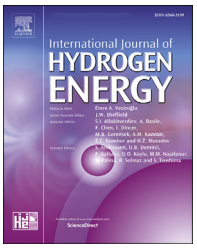

Gas Switching Reforming for syngas production with iron-based oxygen carrier-the performance under pressurized conditions

Ambrose Ugwu [a,*], *Abdelghafour Zaabout* [b], *Julian R. Tolchard* [b], *Paul Inge Dahl* [b], *Shahriar Amini* [a,b,**]

[a] *Norwegian University of Science and Technology, Trondheim, Norway*
[b] *SINTEF Industry, Trondheim, Norway*

ARTICLE INFO

Article history:
Received 30 November 2018
Received in revised form
21 March 2019
Accepted 22 March 2019
Available online 25 April 2019

Keywords:
Chemical looping
Gas switching reforming
Iron-based oxygen carrier
Hydrogen and syngas production
Natural gas reforming
Carbon capture

ABSTRACT

A four-stage Gas Switching Reforming for syngas production with integrated CO_2 capture using an iron-based oxygen carrier was investigated in this study. The oxygen carrier was first reduced using dry methane, where high methane conversion rate was achieved producing CO_2 and steam. Following the reduction stage is a transition to syngas production in an intermediate stage that begins with partial oxidation of methane while methane cracking dominates the rest of the stage. This results in substantial carbon deposition that gasifies in a subsequent reforming stage by cofeeding steam and methane, contributing to more syngas yield. Some of the deposited carbon that could not gasify during the reforming stage slip to the oxidation stage and get combusted by oxygen in the air feed to release CO_2, thereby reducing the CO_2 capture efficiency of the process. It is in this oxidation stage that heat is being generated for the whole cycle given the high exothermicity nature of this reaction. Methane conversion was found to drop substantially in the reforming stage as the pressure increases driven by the negative effect of pressure on both carbon gasification by steam and on the steam methane reforming. The intermediate stage (after reduction) was found less sensitive to the pressure in terms of methane conversion, but the mechanism of carbon deposition tends to change from methane cracking in the POX stage to Boudouard reaction in the reforming stage. However, methane cracking shows a tendency to reduce substantially at higher pressures. This is could be a promising result indicating that high-pressure operation would remove the need for the reforming stage with steam as no carbon would have been deposited in the POX stage.

Introduction

Fossil energy consumption has steadily increased in recent decades, due to the continuous increase in global energy demand, leading to a rise in CO_2 emission [1]. With the rising concerns of global warming and associated climate change [2], development of affordable, clean and reliable energy sources is of high priority. Natural gas conversion into cleaner energy carrier, such as hydrogen, is seen as one

* *Corresponding author.*
** *Corresponding author.*
E-mail addresses: ambrose.ugwu@ntnu.no (A. Ugwu), abdelghafour.Zaabout@sintef.no (A. Zaabout), julian.tolchard@sintef.no (J.R. Tolchard), paul.dahl@sintef.no (P.I. Dahl), shahriar.amini@sintef.no (S. Amini).
https://doi.org/10.1016/j.ijhydene.2019.03.191

Nomenclature

Abbreviations

BET	Brunauer–Emmett–Teller
BSE	Backscattered Electron
CCS	Carbon Capture and Storage
CFB	Circulating Fluidized Bed
CLC	Chemical Looping Combustion
CLR	Chemical Looping Reforming
EDS	Energy-Dispersive Spectroscopy
GSC	Gas Switching Combustion
GSR	Gas Switching Reforming
GST	Gas Switching Technology
OC	Oxygen Carrier
OXI	Oxidation
POX	Partial Oxidation
PSA	Pressure Swing Adsorption
RED	Reduction
REF	Reforming
SEM	Scanning Electron Microscope
SMR	Steam Methane Reforming
XRD	X-Ray Diffraction

Symbols

$C_{deposition}$	Carbon deposition
$Carbon\_dev$	Carbon deviation
$n_{C\_deposited}$	Mole of C deposited
$n_{C,in}$	Total mole of C fed
$n_{C,out}$	Mole of C at the gas outlet.
$n_{CO,out}$	Mole of CO at the gas outlet.
$n_{CO_2,out}$	Mole of CO_2 at the gas outlet.
$n_{fuel,out}$	Mole of fuel at the gas outlet.
$n_{fuel,in}$	Mole of fuel fed
$n_{fuel,converted}$	Mole of fuel converted
$n_{H_2,out}$	Mole of H_2 at the gas outlet.
γ_{fuel}	Fuel conversion

of the most sustainable options, given its projected 45% increase in global production and demand by 2040 [1]. Steam methane reforming (SMR) process is widely used for industrial conversion of natural gas to syngas ($CO + H_2$), but associated with high CO_2 emissions. This is because fossil fuel combustion is required to supply the heat required for the high endothermic reactions (R1 and R5) of the process. Chemical looping reforming (CLR) has been demonstrated as a promising technology integrating the combustion (for heat supply) and reforming steps into a single process, thereby facilitating CO_2 capture at minimal energy penalty [3–5]. This technology was first applied to combustion for capturing CO_2 [6,7] where the typical configuration consists of two interconnected fluidized bed reactors with a metal oxide (oxygen carrier) circulating between them to transport oxygen from the air to the fuel reactor for oxy-combustion. In this way, a pure CO_2 stream (free of N_2) ready for compression and storage is produced [8,9] (Fig. 1). The low energy penalty of chemical looping relative to other CCS technologies has led to the extension of the principle to other energy-intensive processes such as reforming, through the so-called CLR [3,4]. This process has successfully been demonstrated at lab and pilot scales under atmospheric conditions [10–18].

Traditionally, research on CLR has focused on developing suitable oxygen carriers. It is not surprising that Ni-based oxygen carriers were identified as the best performing, owing to the high catalytic activity of metallic nickel for methane reforming [16–18]. The suitability of other environmentally friendly oxygen carriers, such as Fe–, Mn– and Cu-based has also been investigated [19–28]. Fe-based oxygen carriers have shown acceptable performance, with good selectivity to syngas when reduced from Fe_3O_4 to FeO [19]. Further improvement in reactivity and selectivity to syngas was achieved by doping the Fe-based oxygen carrier (OC) with promotors such as NiO [19]. Fe-based solids oxides such as Ce–Fe and La–Fe have also been reported to exhibit high selectivity of methane conversion to syngas, resulting from the intensification of oxygen mobility occurring in the Fe-based solid oxides [29–31].

Given the necessity of high-pressure operation for maximizing energy efficiency and competitiveness with other CO_2 capture technologies [32], the circulating fluidized bed (CFB) configuration is unlikely to be suitable. Solid circulation between the two interconnected reactors would be difficult to achieve under pressurized conditions given that each reactor should be pressurized independently while fulfilling the essential need for heat and mass balance. Any instantaneous pressure imbalance between the reactors may induce instabilities in solid circulation and could result in large leakages through the sealing devices, thereby increasing explosion risks. To date, only one pilot scale experimental study on pressurized chemical looping combustion (CLC) in an interconnected fluidized bed configuration has been completed [33], despite the predicted benefits of such technology in terms of increased energy efficiency [34]. Apart from these operational challenges, there is additional cost and complexity associated with separation systems like cyclone and loop seals.

Attempts have made in recent years to address these issues, where several reactor configurations with no external solid circulation have been proposed and tested [35–39]. Among these, the "Gas Switching Technology (GST)" has high potential in minimizing the scale-up challenges of pressurized chemical looping. This technology employs a single dense fluidized bed reactor operating under bubbling/turbulent regime and avoids the circulation of solid oxygen carrier by alternating the feeds of the oxidizing and reducing gases to complete the different reactions involved in the chemical looping process while ensuring inherent CO_2 capture (Fig. 1b). The GST technology has been proposed for heat [40,41] and hydrogen production with integrated CO_2 capture [8,9]. Experimental studies have proved ease of operation of this technology under atmospheric and pressurized conditions [8,9,42].

Gas Switching Reforming

The GST technology was extended to methane reforming for syngas production with integrated CO_2 capture, the so-called Gas Switching Reforming (GSR) process, as an alternative to the CLR process that uses the interconnected fluidized bed reactors [8,9]. Similar to CLR (Fig. 2a), the typical GSR cycle

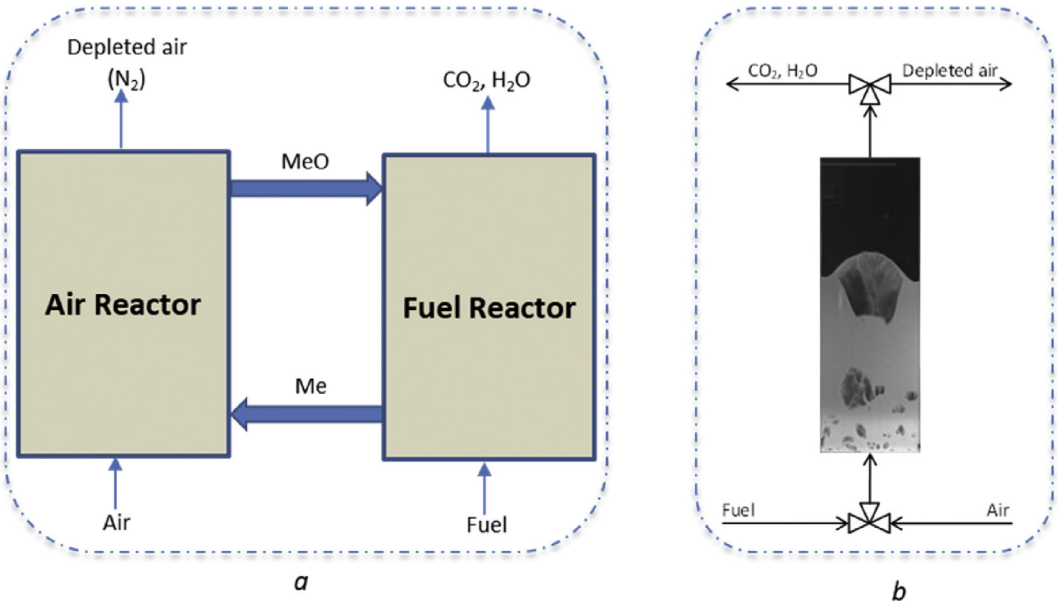

Fig. 1 – Chemical looping combustion. (a: Conventional CLC scheme. b: Simplified GSC scheme).

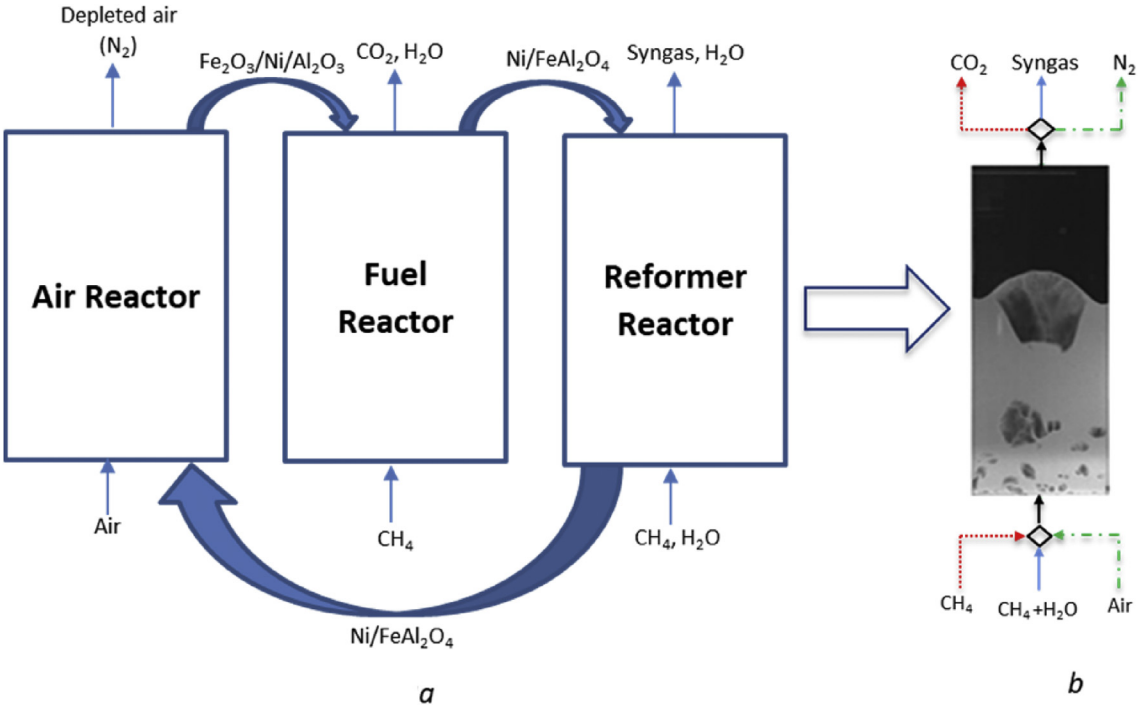

Fig. 2 – Conceptual scheme for autothermal syngas production with integrated CO_2 capture using the three-stages chemical looping reforming technology. (a): Conventional CLR process arrangement and (b): the simplified Gas Switching reforming, GSR, under investigation in this paper.

consists of an air stage where heat for the endothermic reforming reaction is generated through the exothermic oxidation reaction. The heated oxygen carrier is then exposed to a feed of CH_4 in the fuel stage where a simultaneous reduction of the oxygen carrier and methane reforming to syngas take place (Fig. 2b). In this case, the oxygen carrier should also play the role of a catalyst for methane reforming. The major advantage of GSR process is the efficient use of the reaction heat produced during the oxidation stage for the endothermic reforming stage since the reactions occur in a single reactor vessel facilitating autothermal operation of the process [43]. GSR was first demonstrated using a Ni-based oxygen carrier that has shown a very good performance both in the oxidation and reduction stages [8]. This oxygen

carrier exhibited an interesting behaviour in the fuel stage showing two distinct sub-stages, where pure combustion of methane takes place in the first one (oxygen carrier reduction), while pure selectivity to syngas takes place in the second. This behaviour opens the possibility for feeding PSA-off gases to the reduction sub-stage, thereby maximizing fuel.

Conversion in the GSR process [26] . Another benefit of the use of PSA-off gases in the reduction sub-stage of GSR is the exothermicity of H_2 and CO reactions with the oxygen carrier, that reduces the temperature variation in the GSR cycle, thereby resulting in improved fuel conversion [8]. The three-stage GSR configuration, using CO in the reduction stage, CH_4 in the reforming and air in the oxidation stage was also demonstrated experimentally [8]. GSR process through a four-stages configuration has also been proposed (Fig. 3) with the major reactions at different stages shown in Fig. 4. Like other gas switching concepts, GSR faces a challenge from undesired mixing when switching the inlet feed gases, which causes some N_2 to leak into the fuel stage and some CO_2 to escape to the atmosphere with the depleted air. This leakage is small for reforming concepts though; for example, reactor modeling in a previous study on GSR showed that 97% CO_2 capture could be achieved despite this undesired mixing [26] .

The behaviour of GSR using three Fe-based oxygen carriers, supported on commercial alumina (Fe–Al_2O_3, Fe–Ce–Al_2O_3 and Fe–Ni–Al_2O_3), has recently been investigated [44] . The three of them have shown very distinct reduction and reforming stages, similar to the pure Ni-based oxygen carrier tested previously [8], with high conversion of methane to CO_2 in the reduction. As expected, the Fe–Ni–Al_2O_3 outperformed in the reforming showing methane conversion to syngas close to equilibrium at 800–850 °C. The oxidation and reduction mechanisms of the oxygen carrier with Fe–Al_2O_3 have been found to follow **R.1** and **R.2** (see Fig. 4) as revealed by XRD analysis [44] . The phases present after reduction are solid solutions of spinel structured oxides of the general form M_3O_4, where M = Fe, Ni, or Al. In all these phases, iron was present as Fe^{2+} or as a mixture of Fe^{2+} and Fe^{3+} with no evidence of presence of standalone FeO, NiO or metallic Fe or Ni.

For the Ni-free Fe-based oxygen carrier, steam methane reforming occurs following heterogeneous gas-solid reactions. The highly reduced oxygen carrier particles are oxidized by steam and CO_2 to form H_2 and CO (**R.5** to **R.9**) as shown in Fig. 4; the oxidized sites immediately reduces with the incoming CH_4 to result in a steady state steam reforming that can continue indefinitely as long as heat is supplied to drive the overall endothermic reaction system [44] . As for Fe-Ni-Al_2O_3, it is likely that steam methane reforming mainly occurs following reactions **R.6** and **R.7** (Fig. 4), due to the presence of nickel [44] after the oxygen carrier is sufficiently reduced to $NiFeAl_2O_4$ (the XRD data of the reduced Fe–Ni–Al_2O_3 is shown in Fig. 5.

This study further investigates the GSR with the NiO promoted oxygen carrier, Fe–Ni–Al_2O_3, developed and tested in Zaabout et al., 2018 [44] with the focus on the effect of the operating pressure. The prospects of exploiting methane cracking mechanism **R.4** (Fig. 4), in hydrogen production with integrated CO_2 capture through GSR is also explored in this study through a four-stages GSR process (Fig. 3). In addition to the introduction and conclusion sections, this paper has two other main sections: i) experimental set-up ii) results and discussion.

Experiment and methods

Experimental setup

A fluidized bed reactor used for the GSR experiment consists of a cylindrical column (5 cm in inner diameter and 50 cm in

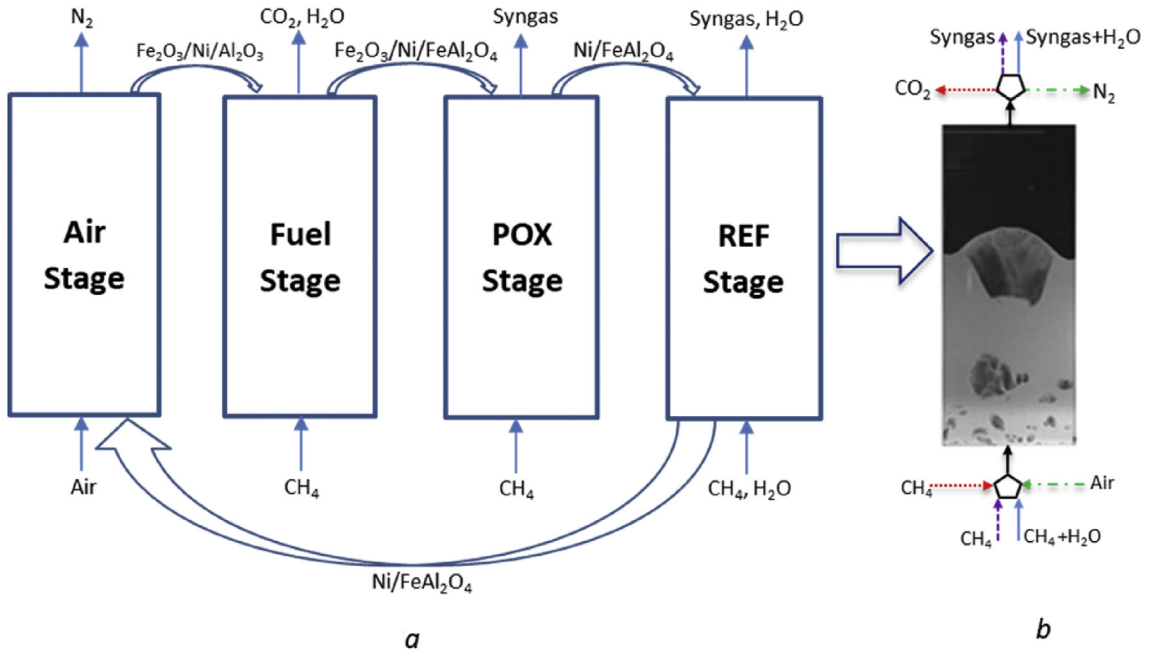

Fig. 3 – Proposed 4-stage configuration of autothermal syngas production with integrated CO_2 capture using a four-stages chemical looping reforming technology. (a) Conventional CLR process arrangement and (b) The simplified Gas Switching Reforming, GSR, under investigation.

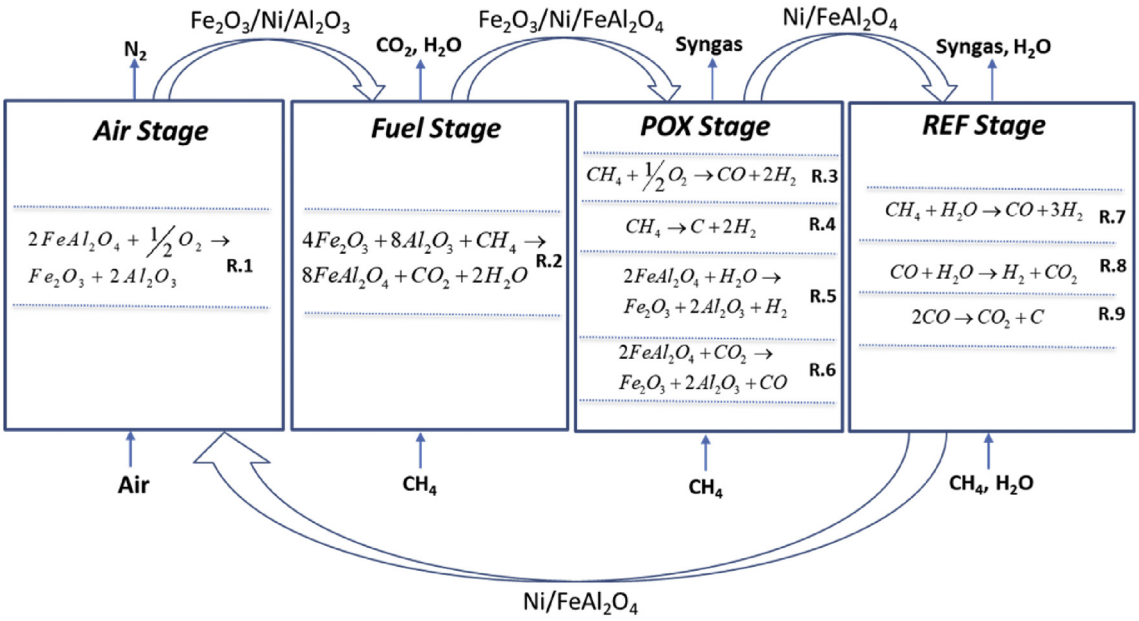

Fig. 4 – The major reactions at different stages of a four-stage chemical looping reforming technology under investigation.

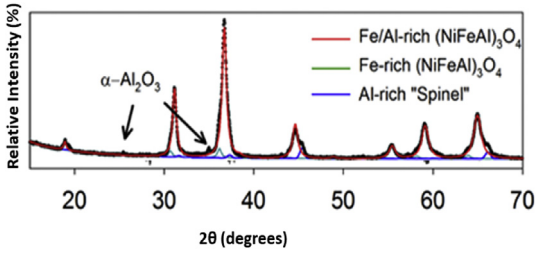

Fig. 5 – Fitted XRD data of the sample (Fe–Ni–Al_2O_3) after 30 min final stage reduction at 800 °C [46].

height) and a freeboard zone as shown in Fig. 6. A fluidized bed is desired to achieve good mixing and temperature distribution [45–47] . The freeboard zone consists of an expanding conic zone (from 5 cm in the lower end diameter to 10 cm at the top end) followed by a cylindrical part to minimize particles entrainment. The total height of the reactor, including the body and the freeboard, is 90 cm. The reactor vessel was made of Inconel 600 to withstand high-temperature gas-solids reactive flows (up to 1000 °C). A porous plate with 20 μm mean pore size and 3 mm thickness, made from Inconel 600, was used as a gas distributor. Heating was done externally through electrically heating elements wound round the reactor vessel to heat up the reactor to a target temperature before starting autothermal GSR process. 25 cm thick insulation was applied to the reactor, combining blankets and vermiculate. The reactor was designed to operate at elevated pressures (up to 10 bar) and was pressurized using a back-pressure valve. Mass flow controllers from Bronkhorst BV were used for feeding gases to the reactor. A three-way electrical valve was used to separate the air and fuel feeds, and to switch between them for cycling reducing and oxidizing conditions in the reactor. A cooler was installed at the outlet of the reactor to cool down the stream of hot gases before sending it to the vent. The gas composition was measured using ETG syngas analyzer connected to the outlet gas stream. The analyzer can sample gases only under atmospheric pressure, which means that in our case the gas had to be sampled after the back-pressure valve. It is necessary to mention that the setup does not allow direct measure steam due to condensation in the heat exchanger. However, the quantity of steam could be quantified through H_2 balance. The temperature was measured at two positions in the reactor, 2 cm and 20 cm above the gas distributor using two thermocouples inserted through the middle axis of the reactor. All the measurement instruments and flow controlling devices were controlled through a LabVIEW application. The LabVIEW application was also used for data acquisition and storage.

Oxygen carrier

Spherical gamma-alumina particles from Sasol (Puralox SCCa 150/200) were applied for wet impregnation of concentrated aqueous ammonium iron(I) citrate solution (~50 g/100 g water) aiming to form nanostructured iron oxide inside the mesoporous alumina structure after heat treatment. The iron precursor was partly substituted by nickel(II) nitrate hexahydrate to form iron oxide-nickel oxide composite structure. Homogenous distribution of the active metal oxides throughout the porous particles was obtained by wet impregnation with subsequent drying steps at 120 °C after each step up to a theoretical loading of ~10 wt% metal oxide, followed by heat treatment for 5 h at 500 °C (60 °C/h) in ambient air. This procedure was repeated until a theoretical loading of the active elements (Fe and Ni) was 1:1 by weight compared to Al in the porous alumina structure. The theoretical Fe:Ni ratio were 2:1 by weight. After the final impregnation and heat treatment steps, the produced particles were sieved (100 μm) to remove fines prior to further analysis and testing. The particle size distribution range was 100–450 μm.

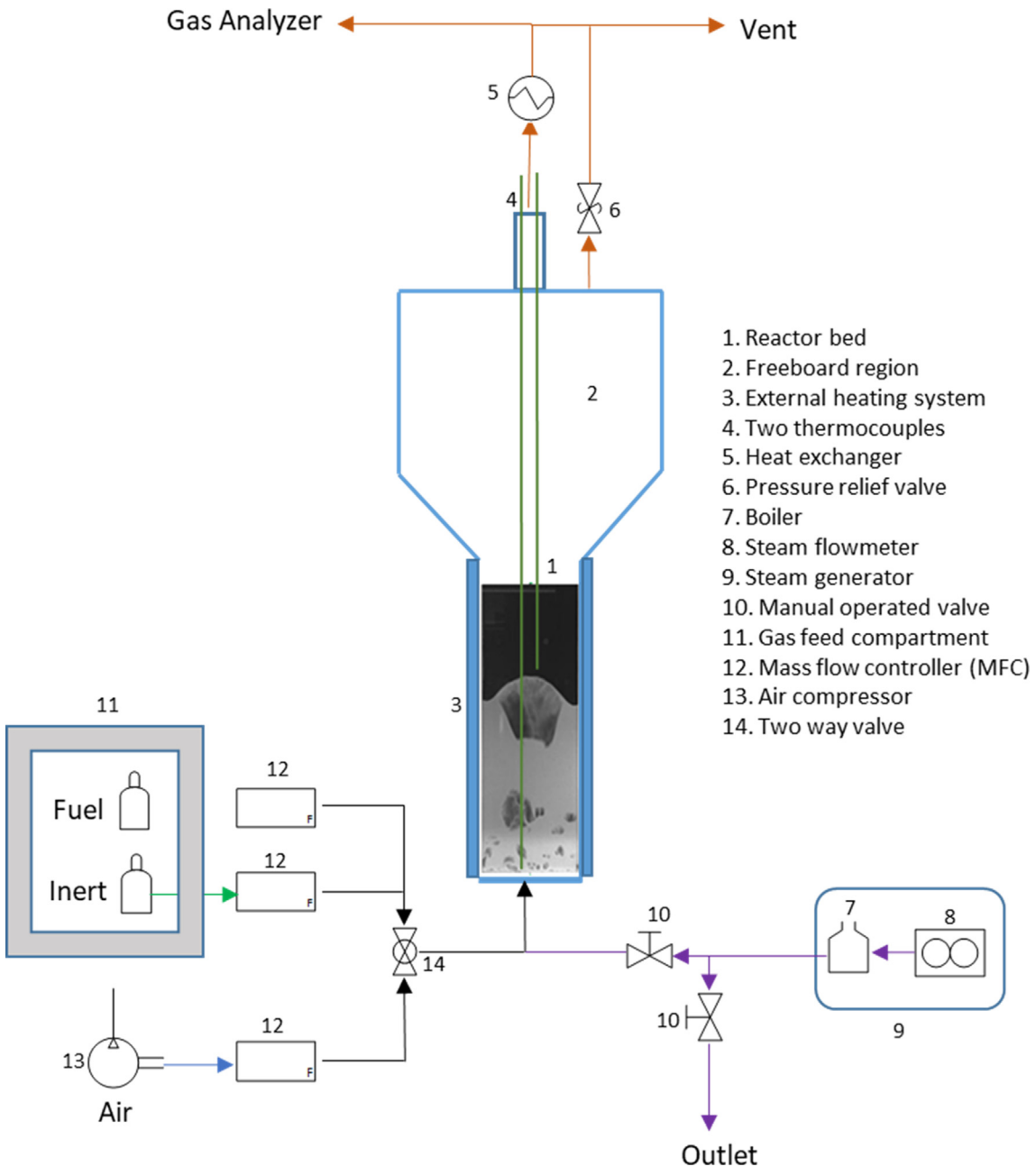

Fig. 6 – GSR Experimental setup.

SEM/EDS analysis on particles after sieving indicated a homogenous distribution of the Fe and Ni throughout the porous alumina structure, as seen in Fig. 7 respectively. The measured loading of active elements (Fe + Ni): Al ≈ 0.8:1 by weight which is slightly lower than the aimed value of 1:1. This reflects the loss of active material by sieving, in form of fines which are loosely deposited on the surface of the particles. The Fe:Ni ratio was found to be ~2:1, as anticipated. The BET surface areas of the produced Fe–Al_2O_3 and Fe–Ni–Al_2O_3 impregnated particles were measured to 102.9 and 97.2 m^2/g, respectively. In comparison, the bare alumina support particles had a BET surface area of 206.0 m^2/g.

Methodology

The GSR concept operates in a cyclic mode by alternating air and fuel feeds to the reactor. During the experiment, various gas was fed to carry out reduction, reforming and oxidation reactions in a bubbling fluidized bed of solid oxygen carrier to produce syngas and pure CO_2 ready for storage or further

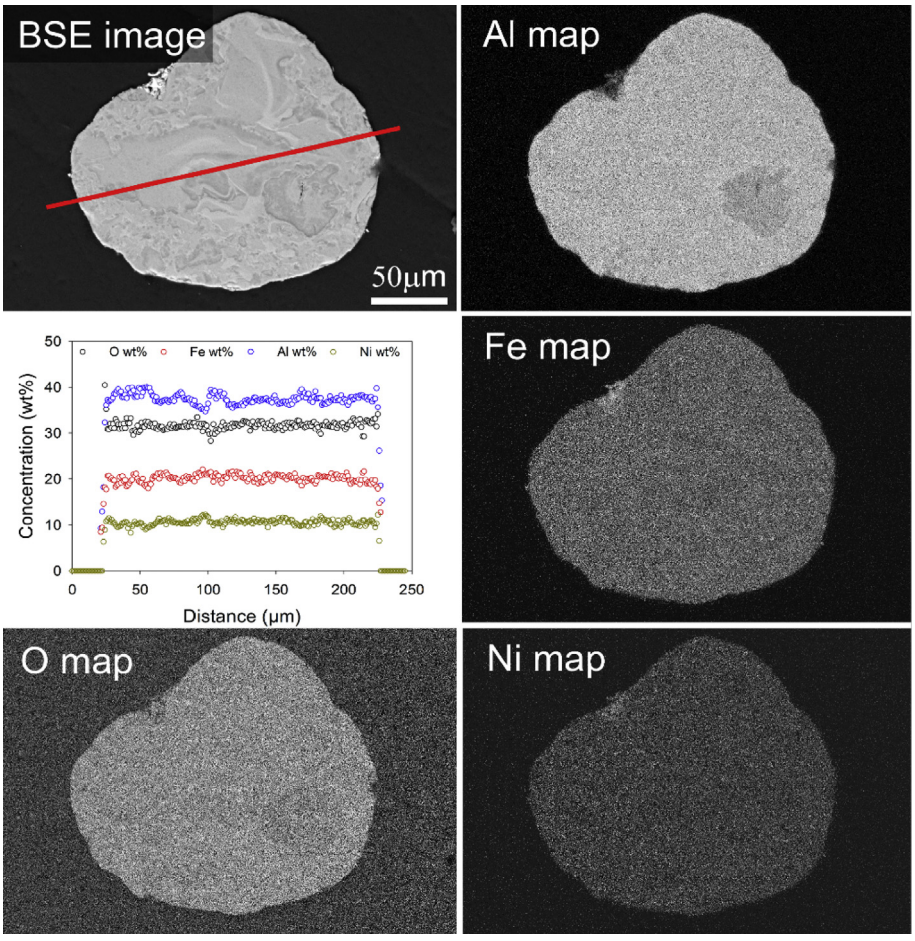

Fig. 7 – Backscattered Electron (BSE) image of a catalyst carrier cross section with corresponding x-ray element maps and quantitative line scan data. The linescan data was collected along the red line indicated on the BSE image. (For interpretation of the references to colour in this figure legend, the reader is referred to the Web version of this article.)

utilization at the fuel stage. A fluidized bed was used to ensure good heat transfer and manage thermodynamic equilibria constraints [48] . About 300 ml of the oxygen carrier was placed initially in the reactor.

The GSR experiments were performed at different operating pressures ranging from 1 to 5 bar at 800 °C. Three-stage process (reduction, reforming and oxidation stage) was designed as explained in section Gas Switching Reforming to complete a redox cycle. The cycle starts with the reduction stage where 0.8–4 nl/min of CH_4 was fed into the reactor between 12 and 2.4min to reduce the $Fe_2O_3/Ni/Al_2O_3$ oxygen carrier for the catalysis of the steam methane reforming and other competing reactions as shown in **R.5** to **R.9** (Fig. 4). After the reduction stage, the reforming stage starts through a combination of catalytic reforming and other heterogeneous reduction reactions to produce syngas (CO and H_2). A feed of air follows to oxidize back the reduced oxygen carrier following an exothermic reaction that builds up heat in the reactor. The generated heat is then being used in the subsequent fuel stage with mainly endothermic reactions (reduction and reforming). Five seconds purging with inert gas is applied between the air and fuel stages to avoid direct contact between them in the feed pipes, thereby eliminating the risk of explosion. Experiments for each operating condition were completed for at least ten redox cycles to ensure repeatability.

As mentioned earlier, real-time temperature and pressure measurements were collected using a Labview application while the online gas composition was measured using an ETG Syngas analyzer. The reactor performance at different temperature was evaluated using the following measures: fuel conversion, CO and H_2 selectivity (expressed as H_2/CO and H_2/C ratios), degree of carbon deposition, as described in next section. These performance measures are defined as specified in Eqs. (1)–(5). The experimental results were compared with equilibrium predictions.

Reactor performance measures

The objective of the GSR process is to convert a hydrocarbon fuel (CH_4 in this study) to syngas (H_2 and CO). Therefore, it is desired to maximize the fuel conversion in the reduction stage, maximize CH_4 conversion at the in all stages. Thus, fuel conversion is an important measure to evaluate the performance of GSR process. This can be quantified as follows:

$$\gamma_{fuel} = 1 - \frac{n_{fuel,out}}{n_{fuel,in}} \quad (1)$$

CO and H_2 are the major constituents of syngas that determine the quality and possible usage of syngas. It is therefore important to determine the syngas (H_2:CO) ratio as:

$$\frac{H_2}{CO} = \frac{n_{H_2,out}}{n_{CO,out}} \quad (2)$$

Significant carbon deposition could block the active sites of the oxygen carrier thereby leading to a drop in activity. The deposited carbon would be released in the oxidation stage in the form of CO_2. Carbon deposition is therefore and important performance measure and can be quantified as:

$$C_{deposition} = \frac{n_{C\_deposited}}{n_{fuel,converted}} = \frac{n_{C,in} - n_{C,out}}{\gamma_{fuel} * n_{fuel,in}} \quad (3)$$

Knowing the mechanism (methane cracking or Boudouard reaction) responsible for carbon deposition is important for process improvement. These mechanisms could be identified using H_2/C ratio. High H_2/C ratio (>2.5) indicates that carbon deposition is mainly through methane cracking and vice versa.

$$\frac{H_2}{C} = \frac{n_{H_2,out}}{n_{CO_2,out} + n_{CO,out}} \quad (4)$$

The deposited carbon in the previous stage would gasify in presence of steam thus increasing syngas yield. This phenomenon was quantified using carbon deviation as described in Eq. (5). The parameter is deduced from carbon balance with negative values indicating gasification phenomenon while positive values indicate no gasification.

$$Carbon\_dev = \frac{n_{C,in} - n_{C,out}}{n_{C,out}} = \frac{n_{C,in}}{n_{C,out}} - 1 \quad (5)$$

Results and discussion

The behaviour of the GSR concept

A three-stages (reduction, reforming and oxidation) cycle was designed to demonstrate the GSR using Fe–Ni/Al_2O_3 oxygen carrier at 1 bar and 800 °C as shown in Fig. 8. The cycle starts with the reduction stage where dry CH_4 is fed to reduce the oxygen carrier, showing high CH_4 conversion (~97.61% close to equilibrium prediction) with a significant yield of CO_2 over several repeatable cycles. As CH_4 conversion starts to drop at the end of the reduction stage, steam is co-fed with CH_4 to start the reforming stage, showing an immediate positive effect by increasing back CH_4 conversion (beyond 90%) to syngas (H_2 and CO) instead of CO_2 as was happening in the reduction stage. CO_2 yield in this stage indicates the presence of water-gas shift reaction. Given that the reactions in both the reduction and reforming stages are endothermic and limited by equilibrium, it is necessary that the reforming stage is followed by an exothermic oxygen carrier oxidation stage with air feed, to provide the heat required for CH_4 conversion in the consecutive stages. The oxygen conversion is complete almost in the entire oxidation stage. A switch to the consecutive reduction stage is applied just after O_2 breakthrough (indicating complete oxidation of the oxygen carrier) to ensure maximal heat usage by the endothermic reforming and reduction reactions. Any further feed of air after O_2 breakthroughs leads to heat removal from the system.

It could, however, be observed that CO_2 is generated in the air stage, indicating the presence of deposited carbon from the precedent stage that combusts with O2 in this stage producing CO_2. The estimated total carbon deposition that leaks to the atmosphere in the air stage is ~1.1% of the total converted methane in the entire fuel stage (both reduction and reforming stages). Note that no carbon deposition has been detected when steam was co-fed with CH_4 in the reduction stage as also observed in the previous work [44]. Carbon deposition through methane cracking was identified as one of the main mechanisms involved in both Fe_2O_3 and Fe_3O_4 reduction with methane, leading to high hydrogen yield [49]. To explore the prospects of exploiting the methane cracking mechanism in producing hydrogen, the feed of dry methane in the reduction stages has been prolonged, before co-feeding steam. Interestingly, an additional distinct stage appears between the reduction and reforming stages (Fig. 9) where methane conversion improves back after it slows down at the end of the reduction stage, but towards syngas in this intermediate stage, rather than CO_2. In this stage, the H_2/C ratio starts at values close to 2, indicating that syngas production begins through partial oxidation of methane **R.3** (Fig. 4), but it rapidly increases to reach a value of ~7 at the end of the stage, indicating that the syngas production mechanism quickly shifts to methane cracking. This is also confirmed by the transient carbon deposition showing a sharp increase in this intermediate stage. Note that methane conversion gradually decreases when methane cracking starts taking over but it remains much higher than the level obtained at the end of the reduction stage.

Mass balance calculation was completed for the reaction of CH_4 with Fe_2O_3/NiO to CH_4 and H_2O (assuming an ideal scenario where NiO reduces to Ni while Fe_2O_3 reduces to $FeAl_2O_4$ as shown by XRD analysis depicted in Fig. 5). For a mass of 296 g of the Fe–Ni–Al_2O_3 oxygen carrier, with an active content of 35 wt% (11.5 wt. NiO and 23.5 wt. Fe_2O_3), the total moles of Fe_2O_3 available for the reaction is ~0.44 mol and for NiO is ~0.46 mol. For a CH_4 feed rate of 0.8 Nl/min ~410 s is needed to fully convert Fe_2O_3 to FeO (when full methane conversion is assumed). It can, however, be seen in Fig. 9 that the reduction stage with full selectivity to CO_2 is finished after only 205 s of reduction time, then syngas starts been produced. With the achieved 90% methane conversion rate in the reduction stage, only ~45% of available active content was consumed in the reduction stage, while the rest remains available for the subsequent partial oxidation (POX) and reforming stages. So, in principle, enough oxygen remains available for fully converting the fed methane in the POX stage through the partial oxidation of methane, but the results show that methane cracking overtakes instead. It is likely that the 50% reduced sites on the oxygen carrier were enough to ignite methane cracking.

An immediate sharp drop in the H_2/C ratio occurs (reaching values close to 2) when steam is co-fed with CH_4 after the intermediate stage, combined with a large improvement in methane conversion (Fig. 10). Interestingly, the transient carbon imbalance (Eq. (5)) is negative in this reforming stage,

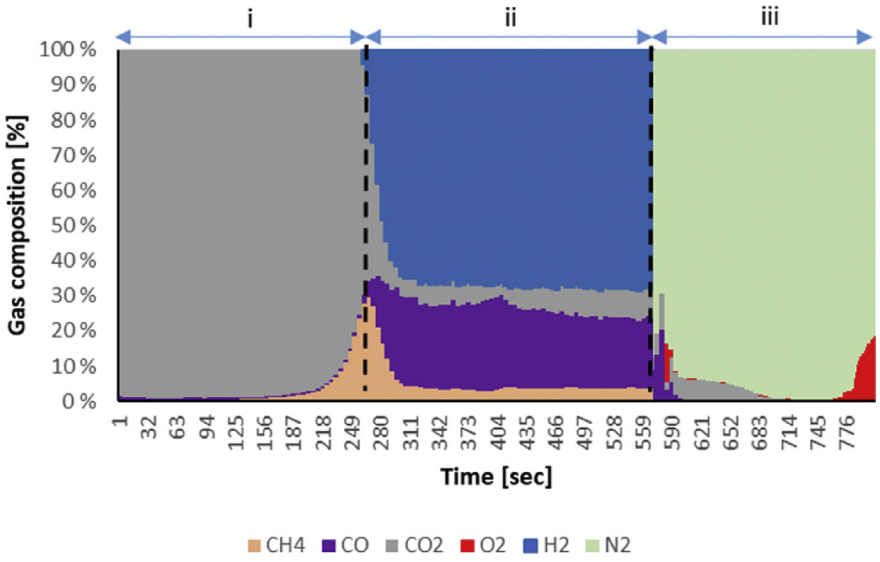

Fig. 8 – The transient dry gas composition at the reactor outlet and H_2/C ratio for a GSR cycle without partial oxidation stage at atmospheric pressure and 800 °C. The GSR stages (reduction, reforming and oxidation) are numbered i, ii and iii respectively.

indicating the existence of a second source of syngas production, which is gasification of carbon that has deposited in the previous stage, by the steam co-fed with methane. This carbon imbalance shows above 30% contribution of carbon gasification in the first third of reforming time but reduces to below 10% thereafter, reflecting that steam methane reforming is becoming the dominating mechanism in syngas production. This is confirmed by the H_2/CO ratio that follows the same trend as the carbon imbalance, showing values ~2 in the first third of reforming time (high contribution of carbon gasification by steam) but increases gradually and stabilizes at ~4 in the rest of the stage (methane reforming domination). CO_2 concentration starts very low in the reforming stage showing a gradual increase, then plateaus as carbon gasification slows down, which is likely originating from the water-gas-shift reaction between the steam supplied and the produced CO. The overall CH_4 conversion in this reforming stage was however lower than the case without the intermediate POX stage (Fig. 11). It could be speculated that the high amount of carbon deposition on the oxygen carrier surface increases the resistance to gas diffusion to the catalytic sites of the oxygen carrier, leading to a reduced methane conversion.

In short, a large contribution of carbon gasification to syngas production occurs first when steam is co-fed with

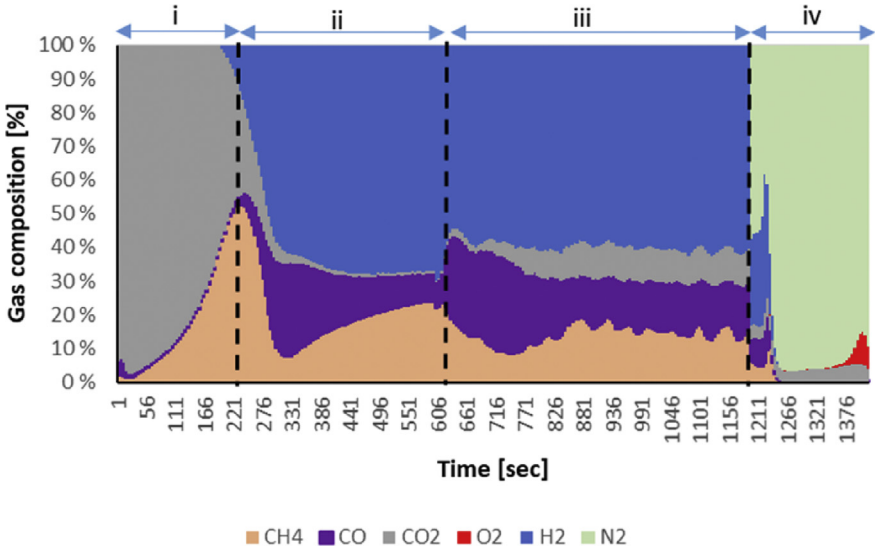

Fig. 9 – The transient dry gas composition at the reactor outlet of a GSR cycles with partial oxidation stage at atmospheric pressure and 800 °C. The GSR stages (reduction, partial oxidation, reforming and oxidation) are numbered i, ii, iii and iv respectively.

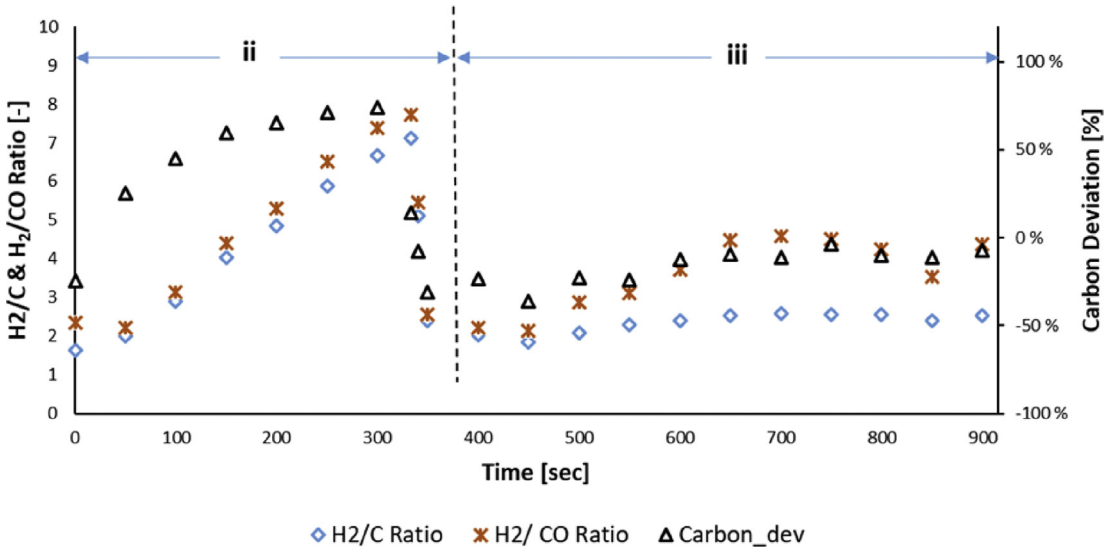

Fig. 10 – The transient H_2/C ratio, H_2/CO syngas ratio and Carbon deviation during the POX and Reforming stage of a GSR cycle at atmospheric pressure and 800 °C. The GSR stages (partial oxidation and reforming) are numbered ii and iii respectively.

methane, then steam methane reforming dominates. The integral of the carbon balance shows that almost 100% of the total carbon deposited in the POX intermediate stage gasifies with steam in the reforming stage (Fig. 12). Some of the deposited carbon is found to combust in the oxidation stage. This implies that some carbon deposition has happened already in the reduction stage with dry methane. Longer reforming stage or an additional separate stage with only steam feed could be applied to fully remove the carbon before the air stage if high CO_2 capture efficiency is targeted. The heat balance is, however, an important factor to take in consideration when designing such a cycle targeting autothermal operation.

Overall, better total methane conversion was achieved in GSR configuration with the only reduction and reforming stage, with lower H_2/CO ratio and minimal carbon deposition (Fig. 11). Moreover, given that the different mechanisms involved in syngas production through methane (SMR, POX, methane cracking) are affected differently by the operating pressure, the sensitivity study to the pressure was completed on the four-stages GSR cycle. This is especially important, given the well-known negative effect of pressure on steam methane reforming reaction (R.7 as shown in Fig. 4) limited by equilibrium. As shown in Appendix 1, very high operating temperatures will be needed with the three-stages GSR process when high-pressure operation is targeted. Some

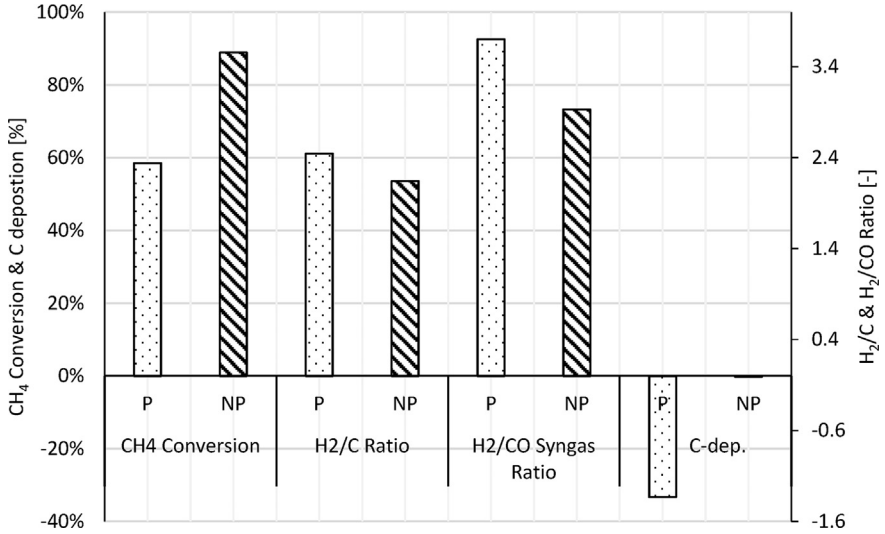

Fig. 11 – Comparison of the performance in the reforming stage (when steam is co-fed with methane) between the case with and without POX at 1 bar and 800 °C. P and NP represent the case with Partial oxidation and without partial oxidation respectively.

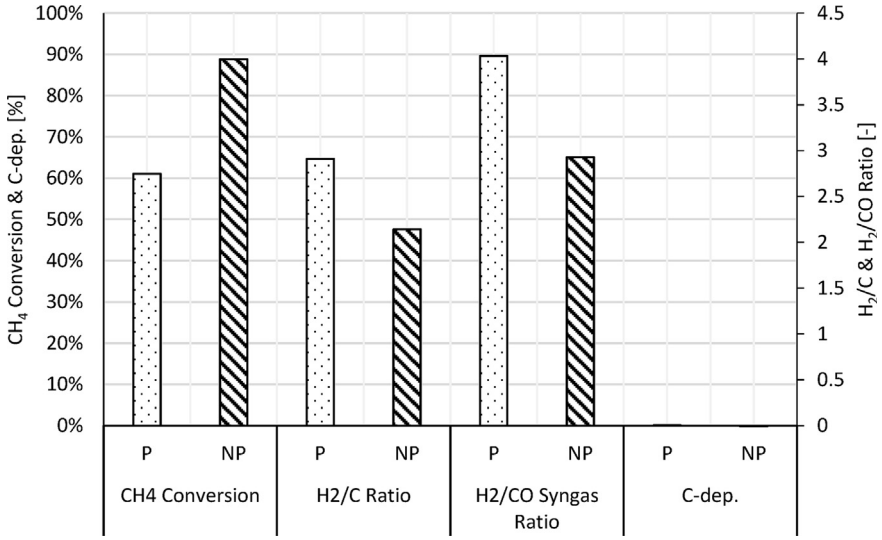

Fig. 12 – Comparison of the performance in the syngas production stage (POX + Ref) between the case with and without POX at 1 bar and 800 °C. P and NP represents the case with Partial oxidation and without partial oxidation respectively.

fundamental differences in the performance between the POX and reforming stages could already be seen at atmospheric pressure with higher methane conversion and higher H_2/CO during the POX stage (Fig. 13).

The effect of pressure

Experiments were completed for operating pressures up to 5 bar. The feed flow rates were increased proportionally to the pressure while the stage time was decreased similarly to maintain the oxygen carrier utilization constant. All experiments were completed at a temperature of 800 °C. In general, methane conversion has a decreasing trend with increased pressure as shown in Fig. 14. This behaviour is consistent with thermodynamics since the overall reaction during the partial oxidation stage and reforming is endothermic. Equilibrium predicts almost complete conversion for all stages up to 5 bar. However, fuel conversion was below equilibrium prediction showing that the process is limited by kinetics. The highest conversion was achieved during the reduction stage, with almost no sensitivity to the pressure, followed by the POX stage and least during the reforming stage (Fig. 14). This could be explained with the increasing endothermicity of the reaction from the reduction to the reforming stage. Pressure increase will thus result in more moles (molecules) per area within the system blocking active sites for reaction (Fig. 14).

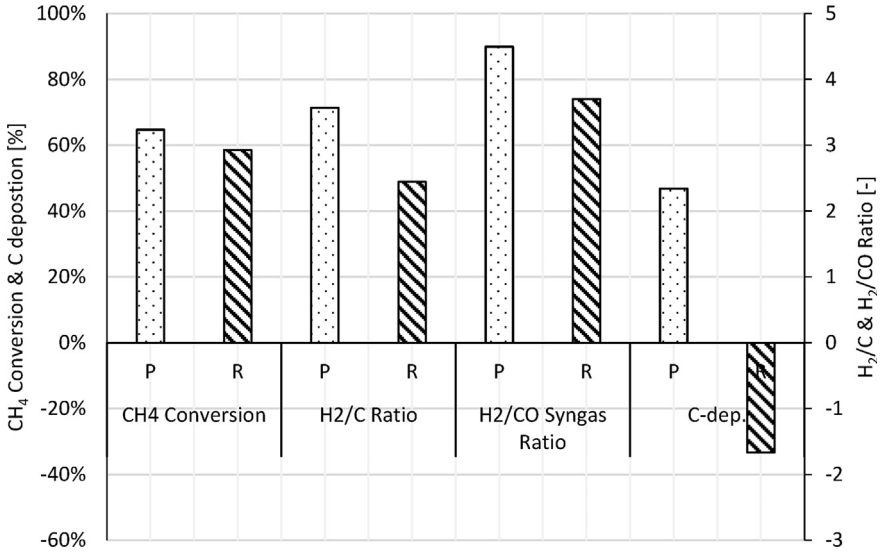

Fig. 13 – Comparison of the performance between the POX and reforming stage for the four-stages GSR cycle (with the intermediate POX case) at 1 bar and 800 °C. P and R represent the POX and the Reforming stages respectively.

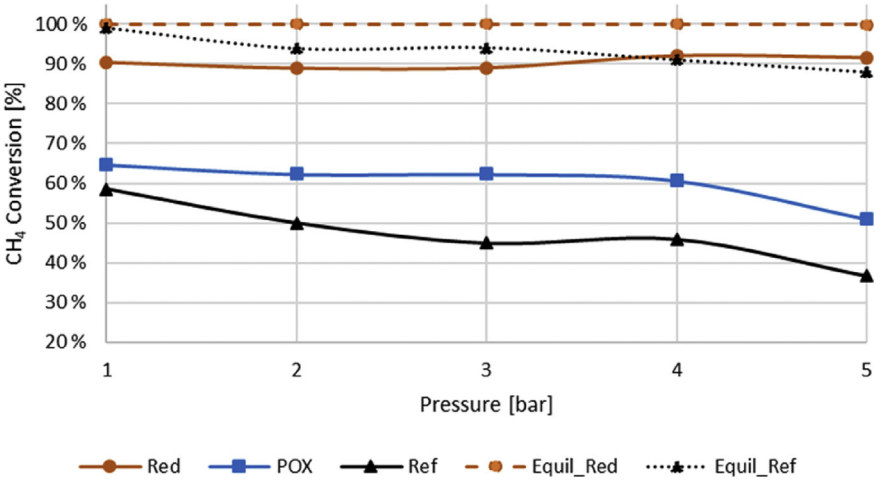

Fig. 14 – Methane conversion at different stages as a function of pressure at 800 °C. Red represents the reduction stage, POX, partial oxidation and Ref, the reforming stage. (For interpretation of the references to colour in this figure legend, the reader is referred to the Web version of this article.)

The effect of pressure is more pronounced for the reforming stage with conversion dropping by approximately 57% by increasing the pressure from 1 bar to 5 bar (Fig. 14).

The H_2/C and H_2/CO ratios reduce with pressure during the POX stage, conforming to thermodynamics as methane cracking reduces with pressure (Fig. 15). The results show however that carbon deposition does not follow the sharp trend shown on the H_2/C and H_2/CO ratios, implying a change in the dominating carbon deposition mechanism from methane cracking to Boudouard. This can be clearly seen on the H_2/CO_2 ratio that decreases sharply from 42 at 1 bar to 6.7 at 3 bar and further down to ~4.8 at 5 bar (Fig. 15). This means that the selectivity to CO_2 rapidly increases at higher pressure driven by the boudouard reaction (**R.9** as shown in Fig. 4).

As for the reforming stage, it was mentioned earlier that at 1 bar the carbon deposited in the POX stage was gasified by the co-fed steam in the subsequent reforming stage, leading to more than 30% excess of syngas production than would have originated from converted methane (Fig. 13). This is concluded from the calculated negative carbon deposition in the reforming stage, interestingly showing gasification of a high percentage of deposited carbon from the previous stage (a slightly longer reforming stage would have led to total gasification of the deposited carbon). The contribution of carbon gasification to syngas production in the reforming stage reduces systematically as the pressure is increased despite the high deposition rate in the previous stage (Fig. 15). This is well in line with the thermodynamic predictions confirming the negative effect of pressure on steam gasification of carbon

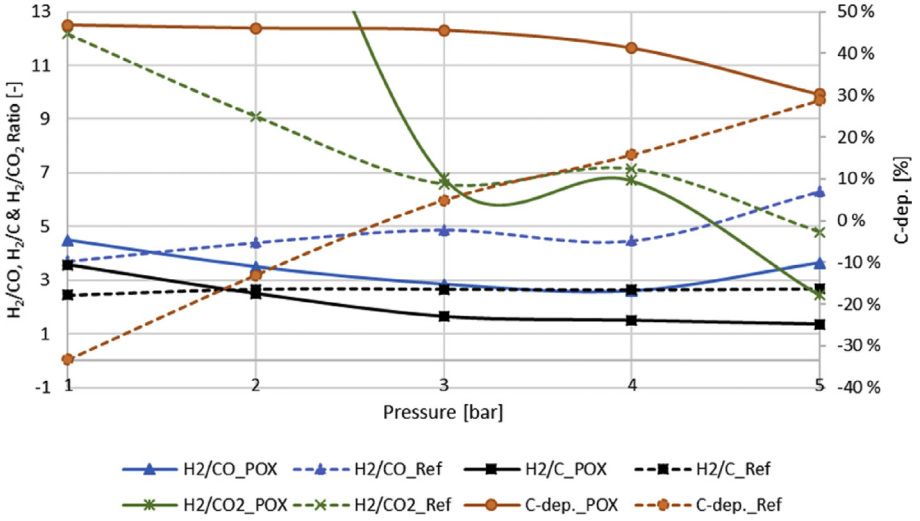

Fig. 15 – Performance (H_2/C ratio, H_2/CO syngas ratio, and carbon deposition) at different stages as a function of pressure at 800 °C. Red represents the reduction stage, POX, partial oxidation and Ref, the reforming stage. (For interpretation of the references to colour in this figure legend, the reader is referred to the Web version of this article.)

[50]. The carbon deposition in the reforming stage becomes positive above 3 bar reflecting the overtaking of the boudouard mechanism over steam carbon gasification as the pressure is further increased. H_2/CO ratio increased with pressure due to the positive influence of pressure on Boudouard and Water-Gas-Shift reactions (Fig. 15). Values beyond 6 were achieved at 5 bar, which could be interesting when hydrogen production is targeted.

The low conversion of methane in this reforming stage combined with the reducing ability in steam gasification of deposited carbon questions the usefulness of combining the POX and reforming stages for syngas production, with integrated CO_2 capture, when high-pressure operation is targeted. However, the reducing carbon deposition in the POX, that accentuates at higher pressures, would remove the need for co-feeding steam in the subsequent stage, making the GSR process even simpler, easier to control and more energy efficient, as steam generation won't be needed. Co-feeding of CO_2 with methane in the POX would also to further suppress carbon deposition by reversing the equilibrium of Boudouard reaction. In this case, the contribution of methane dry reforming to syngas production should be expected due to the presence of CO_2 with methane on reduced Ni. The low H_2/CO ratio achieved in the POX makes the process more suitable for Fischer-Tropsh process; this would be even lower if dry reforming is contributing to syngas production if CO_2 is cofed in the POX. A shift and PSA steps could be applied if H_2 production is targeted.

Future research should focus on investigating the GSR with only the POX stage at higher pressures to confirm the trend of decreased carbon deposition at higher pressures and study the effect of CO_2 co-feeding on the performance in terms of methane conversion, carbon deposition, selectivity to hydrogen and CO and H_2/CO ratio. It is worth mentioning, that a recent study has shown that with a nonstoichiometric CH_4–CO_2 mixture feed (CO_2/CH_4 ratio = 0.38) to a 1 wt% Ni-entrapped Fe_2O_3/Al_2O_3 oxygen carrier at 900 °C, an H_2/CO ratio of 2.09 and high CO selectivity of 96.76% was achieved with minimized carbon deposition [51]. This study was completed at atmospheric pressure.

Conclusion

The performance of a four-stages GSR process for syngas production with integrated CO_2 capture was tested using an iron-based oxygen carrier. The cycle comprises a reduction stage with dry methane (PSA-off gas could also be used), followed by partial oxidation of methane stage (POX), then a reforming stage where steam is fed with methane and finally the oxidation stage for heat production for the whole cycle by the exothermic oxidation reaction. Experiments were completed at 800 °C and pressure ranging from 1–5 bar. The oxygen carrier consisted of a Fe–Ni/Al_2O_3 prepared following impregnation routes. The effective active content of the oxygen carrier was 35 wt.% with one third being NiO and the other two-thirds is Fe_3O_4

High methane combustion rate was achieved in the reduction stage but drops at the end. At the subsequent reforming stage, CH_4 conversion improves to produce CO and H_2 in place of CO_2. At the beginning of the POX stage, syngas was produced through partial oxidation of methane, but shifted gradually to methane cracking, with high H_2/CO ratio ~7 at the end of the stage. This resulted in substantial carbon deposition that was gasified in the subsequent reforming stage by the co-fed steam. With the carbon gasification, syngas yield increased above the estimated amount for the converted methane. Some deposited carbon slipped to the oxidation stage to combust with oxygen in the air feed, thereby reducing the overall CO_2 capture efficiency of the process.

Increase in pressure changed the carbon deposition mechanism in the POX stage from methane cracking to Boudouard, but with limited impact on the overall methane conversion. In parallel, increased pressure reduced the ability of co-fed steam in the reforming stage for gasifying the deposited carbon which consequently magnified the negative effect of pressure on overall methane conversion thus leading to a substantial drop in methane conversion. The overall reduction of carbon deposition observed in the POX stage with increased pressure suggests the possibility of eliminating steam feed in the subsequent reforming stage, thereby maximizing the energy efficiency and reducing the cost associated with steam. It is therefore concluded that when high-pressure operation is targeted, a GSR process with only three stages (RED+POX+OXI) could be best suited for syngas production with integrated CO_2 capture. Future research will explore further opportunities for optimizing the three-stage GSR process at higher pressures.

Acknowledgment

ACT GaSTech project. Project No 271511.

This project has received funding from The Research Council of Norway and is cofounded by the European Commission under the Horizon 2020 programme, The ERANET ACT call; Grant Agreement No 691712. VATL Lab technicians at the Norwegian University of Science and Technology are equally acknowledged for constructing and maintaining the experimental setup.

Appendix 1. Thermodynamic analysis

The equilibrium prediction of different possible reaction paths was performed by minimizing the Gibbs energy function through material balance using non-stoichiometric approach. Fifteen possible reactions have been identified and analysed. The equilibrium predictions were compared with experimental results to identify the dominating reaction path at different GSR stages. The equilibrium calculation was implemented using HSC Chemistry by feeding stoichiometric amounts of the reactants and indicating all the possible products. By minimizing free energy, the equilibrium

composition at 800 °C and pressure between 1 and 5 bar were estimated. Ideal mixture was assumed and the oxygen carrier only in solid phase with the activity coefficient of unity (a pure substance in the condensed phase). Fuel conversion is an important parameter that determines how much fuel required across each stage. Therefore, fuel conversion was estimated following the same assumptions proposed in the article of Svoboda, Slowinski [52].

From the 2nd law of thermodynamics, the expression of the Gibbs free energy at constant temperature and pressure is given as [53].

$$dG|_{T,p} = \sum_{i=1}^{N_{species}} \left[\frac{\partial G}{\partial n_i}\right]_{T,p,n_{j\neq i}} \quad (1)$$

Assuming ideal gas, for minimum Gibbs free energy, $dG|_{T,p} = 0$ for some n. It is also required that the Hessian matrix $(\partial^2 G/\partial n_i \partial n_j)$ is definitely positive. The Gibbs free energy of the reaction is calculated as follows [54]:

$$\Delta G_r = \sum \Delta G_f(\text{final}) - \sum \Delta G_f(\text{initial}) \quad (2)$$

where $\sum \Delta G_f(\text{final})$ is the sum of the Gibbs free energies of the product and $\sum \Delta G_f(\text{initial})$ is the total Gibbs energy of the reactants. The equilibrium constant is then calculated:

$$K^0(T) = \exp\left(-\frac{\Delta G_r^T}{RT}\right) \quad (3)$$

In terms of the partial pressures and activity coefficient, equilibrium constant can be expressed as:

$$K^0 = \frac{\prod (\alpha_{product\ i})^{s_i}}{\prod (\alpha_{reac\ tan\ t\ i})^{s_i}} = \frac{\prod (P_{product\ i})^{s_i}}{\prod (P_{reac\ tan\ t\ i})^{s_i}} \quad (4)$$

where α_i is the chemical activity of the compound i, p is the partial pressure of the gaseous compound i and s_i the stoichiometric coefficient of the compound i.

Reaction 1

$2CO \rightarrow CO_2 + C$

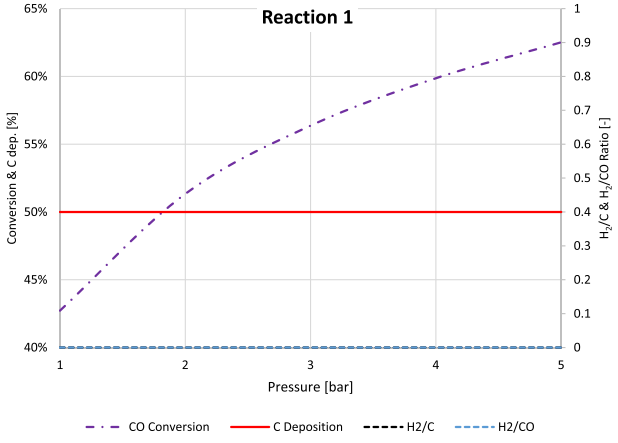

Reaction 2:

Cracking. $CH_4 \rightarrow C + 2H_2$

Reaction 3:

Shift reaction. $CO + H_2O \rightarrow H_2 + CO_2$

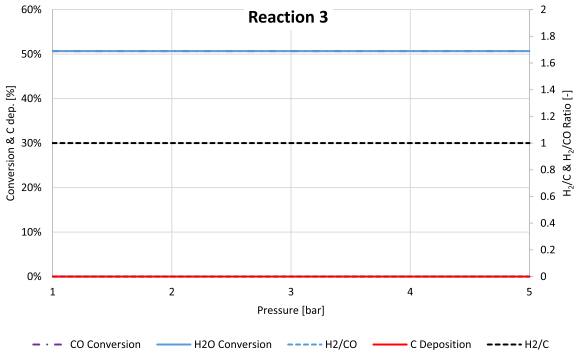

Reaction 4:

SMR. $CH_4 + H_2O \rightarrow CO + 3H_2$

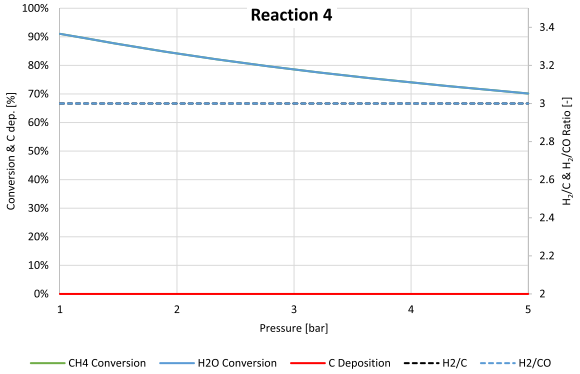

REFERENCES

[1] Nejat P, et al. A global review of energy consumption, CO2 emissions and policy in the residential sector (with an overview of the top ten CO2 emitting countries). Renew Sustain Energy Rev 2015;43:843–62.
[2] Cook J, et al. Quantifying the consensus on anthropogenic global warming in the scientific literature. Environ Res Lett 2013;8(2):024024.
[3] Anthony EJ. Solid looping cycles: a new technology for coal conversion. Indus Eng Chem Res 2008;47(6):1747–54.
[4] Rydén M, Arjmand M. Continuous hydrogen production via the steam–iron reaction by chemical looping in a circulating fluidized-bed reactor. Int J Hydrogen Energy 2012;37(6):4843–54.
[5] Adanez J, et al. Progress in chemical-looping combustion and reforming technologies. Prog Energy Combust Sci 2012;38(2):215–82.
[6] Ishida M, Zheng D, Akehata T. Evaluation of a chemical-looping-combustion power-generation system by graphic exergy analysis. Energy 1987;12(2):147–54.
[7] Lyngfelt A, Leckner B, Mattisson T. A fluidized-bed combustion process with inherent CO2 separation; application of chemical-looping combustion. Chem Eng Sci 2001;56(10):3101–13.
[8] Wassie SA, et al. Hydrogen production with integrated CO2 capture in a novel gas switching reforming reactor: proof-of-concept. Int J Hydrogen Energy 2017;42(21):14367–79.
[9] Wassie SA, et al. Hydrogen production with integrated CO2 capture in a membrane assisted gas switching reforming reactor: proof-of-Concept. Int J Hydrogen Energy 2018;43(12):6177–90.
[10] Kronberger B, et al. A two-compartment fluidized bed reactor for CO2 capture by chemical-looping combustion. Chem EngTechnol 2004;27(12):1318–26.
[11] Linderholm C, et al. 160 h of chemical-looping combustion in a 10 kW reactor system with a NiO-based oxygen carrier. Int J Greenh Gas Control 2008;2(4):520–30.
[12] Johansson E, et al. A 300 W laboratory reactor system for chemical-looping combustion with particle circulation. Fuel 2006;85(10-11):1428–38.
[13] Ding N, et al. Development and testing of an interconnected fluidized-bed system for chemical looping combustion. Chem EngTechnol 2012;35(3):532–8.
[14] Kolbitsch P, et al. Operating experience with chemical looping combustion in a 120 kW dual circulating fluidized bed (DCFB) unit. Int J Greenh Gas Control 2010;4(2):180–5.
[15] Ryden M, Lyngfelt A. Using steam reforming to produce hydrogen with carbon dioxide capture by chemical-looping combustion. Int J Hydrogen Energy 2006;31(10):1271–83.
[16] Rydén M, Lyngfelt A, Mattisson T. Synthesis gas generation by chemical-looping reforming in a continuously operating laboratory reactor. Fuel 2006;85(12-13):1631–41.
[17] de Diego LF, et al. Hydrogen production by chemical-looping reforming in a circulating fluidized bed reactor using Ni-based oxygen carriers. J Power Sources 2009;192(1):27–34.
[18] Proell T, et al. Syngas and a separate nitrogen/argon stream via chemical looping reforming - A 140 kW pilot plant study. Fuel 2010;89(6):1249–56.
[19] Zafar Q, Mattisson T, Gevert B. Redox investigation of some oxides of transition-state metals Ni, Cu, Fe, and Mn supported on SiO2 and MgAl2O4. Energy Fuels 2006;20(1):34–44.
[20] Khan MN, Shamim T. Investigation of hydrogen generation in a three reactor chemical looping reforming process. Appl energy 2016;162:1186–94.
[21] Khan MN, Shamim T. Techno-economic assessment of a plant based on a three reactor chemical looping reforming system. Int J Hydrogen Energy 2016;41(48):22677–88.
[22] Khan MN, Shamim T. Exergoeconomic analysis of a chemical looping reforming plant for hydrogen production. Int J Hydrogen Energy 2017;42(8):4951–65.
[23] Khan MN, Shamim T. Thermodynamic screening of suitable oxygen carriers for a three reactor chemical looping reforming system. Int J Hydrogen Energy 2017;42(24):15745–60.
[24] Cloete S, Khan MN, Amini S. Economic assessment of membrane-assisted autothermal reforming for cost effective hydrogen production with CO2 capture. Int J Hydrogen Energy 2019;44(7):3492–510.
[25] Nazir SM, et al. Gas switching reforming (GSR) for power generation with CO2 capture: process efficiency improvement studies. Energy 2019;167:757–65.
[26] Nazir SM, et al. Techno-economic assessment of the novel gas switching reforming (GSR) concept for gas-fired power production with integrated CO2 capture. Int J Hydrogen Energy 2018;43(18):8754–69.
[27] Nazir S, Bolland O, Amini S. Analysis of combined cycle power plants with chemical looping reforming of natural gas and pre-combustion CO2 capture. Energies 2018;11(1):147.
[28] Nazir SM, Bolland O, Amini S. Full plant scale analysis of natural gas fired power plants with pre-combustion CO2 capture and Chemical Looping Reforming (CLR). Energy Procedia 2017;114:2146–55.
[29] Li KZ, et al. Transformation of methane into synthesis gas using the redox property of Ce-Fe mixed oxides: effect of calcination temperature. Int J Hydrogen Energy 2011;36(5):3471–82.
[30] Zhu X, et al. Chemical-looping steam methane reforming over a CeO2-Fe2O3 oxygen carrier: evolution of its structure and reducibility. Energy Fuel 2014;28(2):754–60.
[31] Zheng Y, et al. Designed oxygen carriers from macroporous LaFeO3 supported CeO2 for chemical-looping reforming of methane. Appl Catal B: Environ 2017;202:51–63.
[32] Hamers HP, et al. Comparison on process efficiency for CLC of syngas operated in packed bed and fluidized bed reactors. Int J Greenh Gas Control 2014;28(0):65–78.
[33] Xiao R, et al. Pressurized chemical-looping combustion of coal using an iron ore as oxygen carrier in a pilot-scale unit. Int J Greenh Gas Control 2012;10:363–73.
[34] Adanez J, et al. Progress in chemical-looping combustion and reforming technologies. Prog Energy Combust Sci 2012;38(2):215–82.
[35] Zaabout A, et al. Experimental demonstration of a novel gas switching combustion reactor for power production with integrated CO2 capture. Ind Eng Chem Res 2013;52(39):14241–50.
[36] Noorman S, van Sint Annaland M, Kuipers. Packed bed reactor technology for chemical-looping combustion. Ind Eng Chem Res 2007;46(12):4212–20.
[37] Hamers HP, et al. A novel reactor configuration for packed bed chemical-looping combustion of syngas. Int J Greenh Gas Control 2013;16(0):1–12.
[38] Zaabout A, Cloete S, Amini S. Hydrodynamic investigation into a novel IC-CLC reactor concept for power production with integrated CO2 capture. In: 10th International conference on computational fluid dynamics in the oil & gas, metallurgical and process industries; 2014. Trondheim, Norway.
[39] Osman M, et al. Internally circulating fluidized-bed reactor for syngas production using chemical looping reforming. Chem Eng J 2018.
[40] Zaabout A, et al. Experimental demonstration of a novel gas switching combustion reactor for power production with

integrated CO2 capture. Ind Eng Chem Res 2013;52(39):14241–50.
[41] Nazir SM, et al. Gas switching reforming (GSR) for power generation with CO2 capture: process efficiency improvement studies. Energy 2018.
[42] Zaabout A, Cloete S, Amini S. Autothermal operation of a pressurized gas switching combustion with ilmenite ore. Int J Greenh Gas Control 2017;63:175–83.
[43] Ortiz M, et al. Optimization of hydrogen production by chemical-looping auto-thermal reforming working with Ni-based oxygen-carriers. Int J Hydrogen Energy 2011;36(16):9663–72.
[44] Zaabout A, et al. Gas Switching Reforming (GSR) for syngas production with integrated CO2 capture using iron-based oxygen carriers. Int J Greenh Gas Control 2019;81:170–80.
[45] Agu CE, et al. Investigation of Bubbling Behaviour in Deep Fluidized Beds at Different Gas Velocities using Electrical Capacitance Tomography. Ind Eng Chem Res 2019.
[46] Agu CE, et al. Determination of onset of bubbling and slugging in a fluidized bed using a dual-plane electrical capacitance tomography system. Chem Eng J 2017;328:997–1008.
[47] Abanades JC, et al. Fluidized bed combustion systems integrating CO2 capture with CaO. Environ Sci Technol 2005;39(8):2861–6.
[48] Svoboda K, et al. Thermodynamic possibilities and constraints for pure hydrogen production by iron based chemical looping process at lower temperatures. Energy Convers 2007;48(12):3063–73.
[49] Monazam ER, et al. Kinetics of the reduction of hematite (Fe2O3) by methane (CH4) during chemical looping combustion: a global mechanism. Chem Eng J 2013;232:478–87.
[50] Roberts D, Harris D. Char gasification with O2, CO2, and H2O: effects of pressure on intrinsic reaction kinetics. Energy Fuel 2000;14(2):483–9.
[51] Kang D, et al. Syngas production on a Ni-enhanced Fe 2 O 3/ Al 2 O 3 oxygen carrier via chemical looping partial oxidation with dry reforming of methane. Appl Energy 2018;211:174–86.
[52] Svoboda K, et al. Thermodynamic possibilities and constraints for pure hydrogen production by iron based chemical looping process at lower temperatures. Energy Convers Manag 2007;48(12):3063–73.
[53] Solsvik J, Haug-Warberg T, Jakobsen HA. Implementation of chemical reaction equilibrium by Gibbs and Helmholtz energies in tubular reactor models: application to the steam–methane reforming process. Chem Eng Sci 2016;140:261–78.
[54] Barin I, Platzki G. Thermochem Data Pure Substan 1989;304. Wiley Online Library.